Impurity behavior during sawtooth activity in tokamak plasmas

T. Nicolas, H. Lütjens, J.-F. Luciani, X. Garbet, R. Sabot

Impurity behavior during sawtooth activity in tokamak plasmas

T. Nicolas,[1] H. Lütjens,[2] J.-F. Luciani,[2] X. Garbet,[1] and R. Sabot[1]
[1]*CEA, IRFM, F-13108 Saint-Paul-Lez-Durance, France*
[2]*Centre de Physique Théorique, Ecole Polytechnique, CNRS, F-91128 Palaiseau Cedex, France*

(Received 4 October 2013; accepted 9 December 2013; published online 14 January 2014)

The transport of impurities by a sawtooth crash is simulated with the XTOR-2F code. Impurities are modeled as passive scalars, evolving in the compressible MHD flow inferred from the main MHD plasma. For a peaked impurity density profile, the non-linear kink flow of the sawtooth crash redistributes the profile efficiently and most of the particles in the peak inside the $q=1$ surface are expelled. For an initially hollow impurity density profile, the crash leads to a significant penetration up to the magnetic axis. The results are compared with Kadomtsev's model. Despite essentially different mechanisms, the evolution of the particle content inside the $q=1$ surface for Kadomtsev's model and for the non-linear case are virtually identical for the peaked profile, while the model slightly overestimates penetration for the hollow case. © *2014 AIP Publishing LLC*. [http://dx.doi.org/10.1063/1.4861859]

I. INTRODUCTION

In hot magnetized plasmas, the presence of impurities leads to radiative losses proportional to Z^2, where Z is the charge of the impurity. This is a serious issue for fusion plasmas, especially in machines with tungsten (W) divertor plates, where physical sputtering at the strike points can inject W into the plasma.[1] A maximum relative W concentration of 1.9×10^{-4} can be tolerated in the core of ITER in order to reach the ignition condition.[2] It has been reported[3–7] that sawteeth can help to avoid accumulation of impurities in the core. Although suppression of W accumulation has been achieved in some advanced scenarios,[8] this is an important motivation for carrying out modelling of impurities by sawtooth crashes.

Furthermore, deuterium-tritium fusion reactions produce energetic α particles which contribute to plasma heating. After transferring their power, He ash must be continuously extracted, otherwise fuel dilution causes the fusion efficiency to decrease until the reactions stop. Since the pumps are located under the divertor plates[9] and He is produced in the core, there must be some mechanism to efficiently transport it from the core to the edge of the plasma. Sawteeth have been proposed as a possible mechanism for such a transport[10,11] in the $q < 1$ region, while turbulence is supposed to take over in the $q > 1$ region. Indeed, sawteeth are well-known to flatten the temperature and density profiles, at least to lowest order, resulting in a transient burst of transport.

This work is in part motivated by the experimental observation and numerical confirmation of a significant deviation from flatness of the post-crash density profiles in Tore Supra ohmic plasmas in Ref. 12. The results were recently confirmed by the same observation on the JET tokamak.[13] After the crash, a crescent-shaped structure was observed inside the $q=1$ surface. Despite its small amplitude ($\sim$ 2% of the total density but 10% of the pre-crash peak inside the $q=1$ surface), the presence of this structure raised concern about the efficiency of the sawtooth flushing mechanism. Indeed, should this be a universal feature, it would mean that a significant fraction of the expelled core density is reinjected in the core immediately after the crash, reducing the efficiency of the crash in flushing the core.

In this article, we use sawteeth simulated by the XTOR-2F code[14] to assess impurity transport during the sawtooth crash. The cases of peaked impurity profiles (He-like) and hollow impurity profiles (corresponding to an impurity, e.g., W, generated at the edge and slowly reaching the $q=1$ surface) are investigated. It is shown that as in the case of electron density redistribution, crescent-shaped structures can sometimes be observed, but they have a small amplitude and do not seem to constitute a source of concern for the redistribution by the crash. The results are also compared to a 1-D transport model deduced from Kadomtsev's conservation rules.[15–17] It is emphasized that this model, contrary to conventional wisdom, does not predict flat profiles at the end of the crash.

The XTOR-2F code is capable of simulating stationary self-consistent sawtooth cycles at reasonably high Lundquist number S ($S = \tau_R/\tau_A$, where τ_R is the resistive time and τ_A is an Alfvén time) and with diamagnetic effects. The value used in the simulations is $S = 10^7$, lower than the experimental values for Tore Supra and JET, respectively, $S_{TS} \sim S_{JET} \sim 2\times10^8$ in typical ohmic pulses.

The paper is organized as follows. In Sec. II, the MHD model solved by the XTOR-2F code is recalled. In Sec. III, the equations solved by the impurity species are presented and justified. The modelling results of the impact of the sawtooth crash on impurity transport are presented in Sec. IV. In Sec. V, the results of Sec. IV are compared with a 1D Kadomtsev model. A discussion and a conclusion follow in Secs. VI and VII.

II. THE MHD MODEL

The following set of normalized MHD equations is solved by the XTOR-2F code:

$$\partial_t \rho + \nabla\cdot(\rho\mathbf{v}) = -\mathbf{v}\cdot\nabla p_i - \Gamma p_i \nabla\cdot\mathbf{v}, \quad (1)$$

$$\frac{\partial \mathbf{B}}{\partial t} = S_\rho \nabla\cdot D_\rho \nabla\rho;$$

$$q\,\partial_t \mathbf{v} + \mathbf{v}\cdot\nabla\mathbf{v} + \mathbf{v}_i^{\perp}\cdot\nabla\mathbf{v}_{\perp} = -\mathbf{J}\times\mathbf{B} + \nabla p + \mu\nabla_{\perp}^2\mathbf{v}; \quad (2)$$

$$\partial_t p + \mathbf{v}\cdot\nabla p + Cp\nabla\cdot\mathbf{v} + aC\frac{p}{q}\nabla p_i\cdot\nabla\times\frac{\mathbf{B}}{B^2} = \cdots$$

the simulations at the maximum numerically

$$\nabla\cdot\left(\frac{q\mathbf{v}_{\perp}}{B^2}\nabla\frac{p}{q}\right) + \nabla\cdot\left(\frac{q\mathbf{v}_{jj}}{B^2}\mathbf{B}\cdot\nabla\frac{p}{q}\right) + S_H; \quad (3)$$

$$\partial_t\mathbf{B} = \nabla\times(\mathbf{v}\times\mathbf{B}) + a\nabla\times\frac{\nabla_{jj}p_e}{q} - \nabla\times\eta\mathbf{J}: \quad (4)$$

Here, the magnetic field is normalized to aB_0/R_0, velocities to the Alfvén velocity $V_A = aB_0/(R_0\sqrt{\mu_0 q_0})$, a and R_0 are the minor and major radius of the plasma, and B_0 is the magnitude of $\mathbf{B}$ on the magnetic axis. The pressure is normalized to $q_0V_A^2$, where q_0 is the mass density on the magnetic axis. The density is normalized to q_0/m_i, where m_i is the deuterium mass, and the diffusion coefficients are normalized to a^2/τ_A, with $\tau_A = a/V_A$. The resistivity η is equal to S^{-1} in the centre, where S is the Lundquist number, and the resistivity profile is such that ηj_u = constant radially, with j_u being the equilibrium toroidal current. Also, the parameter $a = V_A/(\omega_{ci}R_0)$, $\omega_{ci} = eB_0/m_i$, characterizes the amplitude of all diamagnetic terms. Note that it is also equal to d_i/R_0, where d_i is the ion skin depth. The variable $\mathbf{v}$ represents the MHD velocity: $\mathbf{v} = \mathbf{E}\times\mathbf{B}/B^2 + v_{jj}\mathbf{i}$, and $\mathbf{v}_i^{\perp} = a/(qB^2)\mathbf{B}\times\nabla p_i$ designates the ion diamagnetic velocity. Thus, the total ion velocity is $\mathbf{v}_{i;tot} = \mathbf{v} + \mathbf{v}_i^{\perp}$. The symbols $\perp$ and jj refer to directions perpendicular and parallel to the magnetic field, i and e to ion and electron populations, S_q and S_H are a particle and heat source, C is the ratio of specific heats, η is the resistivity, and $n = n_i = n_e$ (quasi-neutrality). The fourth term in the l.h.s. of Eq. (1) is the divergence of the diamagnetic flux. Diamagnetic effects account for plasma rotation and are responsible for the real frequency of the kink mode. They also play a crucial role in accelerating reconnection during a sawtooth crash, through the second term in the r.h.s. of Eq. (4).[18,19] When the code is started with a kink unstable equilibrium, different regimes are achievable according to the ratio between the Lundquist number and the amplitude of diamagnetic effects a. For higher S and a values, a regime of self-sustained sawtooth cycles, where the crash is significantly accelerated by diamagnetic effects, can be achieved. We chose to carry out affordable Lundquist number, which is $S = 10^7$. For this value and for the circular equilibrium used in this contribution, the sawtooth cycling regime can be achieved for $a \geq 0.08$. We chose $a = 0.1$ in order to guarantee a sawtoothing regime. Thus, referring to Fig. 6 of Ref. 18, we are in the upper-right domain, denoted "sawtooth cycling." The value used for a is larger than the experimental value for the Tore Supra tokamak by a factor of 2 approximately, since $a_{TS} \sim 0.05$ typically. It is currently possible to operate routinely in the sawtooth cycling regime only at these values, $S = 10^7$ and $a = 0.1$. Increasing both a and S are very challenging numerically since they increase significantly the simulation time, whereas decreasing them leads to entering the "kink cycling" regime where there is no clear timescale separation between the ramp and crash phases. At least in this regard, the sawtooth cycling regime is the one that best reproduces the features of experimental sawteeth. Moderate increase of S and a inside the sawtooth cycling regime would have a moderate effect on the characteristics of the crash: the sawtooth period is roughly proportional to S, whereas the crash dynamics is most sensitive to a in the sawtooth cycling regime. Increasing it accelerates the crash phase,[18] but the basic physical mechanisms at stake remain unchanged.

The other parameters of the circular equilibrium used in this study are as follows: $\beta_p = 0.2$, $a/R_0 = 0.37$, $D_{\perp} = 10^{-7}$, $\nu_{\perp} = 10^{-6}$, and $\mu = 5\times10^{-6}$ in the core, increasing toward the edge, following the resistivity profile.

Fig. 1 represents, for this setup, the kinetic energies and the pressure at $s = 0.1$ and $s = 0.5$, where $s = \sqrt{\psi/\psi_a}$ is the radial coordinate in XTOR-2F, with ψ being the poloidal magnetic flux and $\psi_a = \psi(r = a)$. It is seen that the sawtooth crashes are self-sustained. The kink precursor is also clearly observed in the pressure profile.

III. IMPURITY MODELLING WITH XTOR-2F

To simulate impurity transport by the sawtooth crash, passive scalars are introduced in the simulation. The impurities have no effect on the sawtooth cycle. In other words, impurity radiation and its cooling effect are not taken into account. The feedback on the main plasma will be dealt with in the future by adding a sink term in the pressure equation,

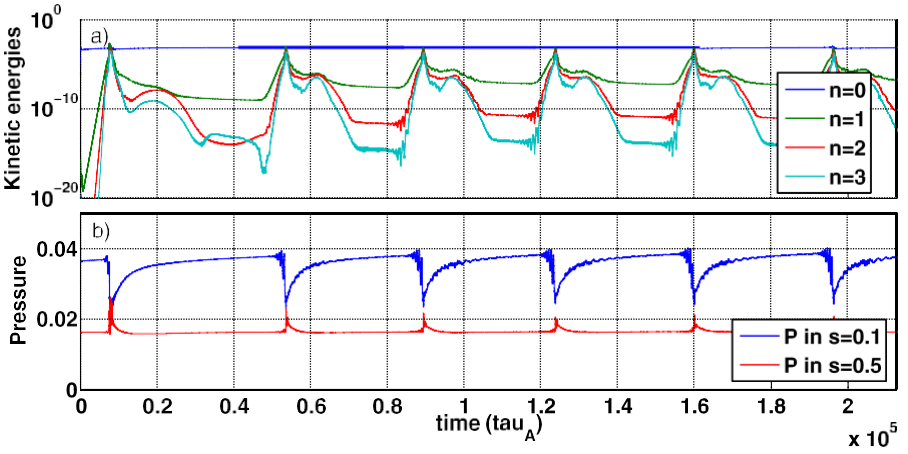

FIG. 1. Kinetic energies of the toroidal modes $n = 0$–3 (a) and central pressure (b) in a sawtooth crash simulation, with $S = 10^7$, $a = 0.1$. A stationary regime of sawtooth cycles can be achieved after a few tens of thousands τ_A.

designed to reproduce the impurity radiation. In this study, however, the mere question of particle redistribution by the sawtooth crash is investigated.

Even though impurities are passive, we do not simulate pure advection. Indeed, simulating pure advection by $v = v_\perp + v_{\parallel} b$ would imply losing particle conservation, since in our simulations $\nabla \cdot v \neq 0$ is a large curvature term. We will also check when we benchmark the impurity model that pure advection is unable to capture the rich behaviour of density during the sawtooth crash. Compressibility must be added, hence the total impurity velocity $v_{Z,tot}$ of an impurity $^{Z}_{A}X$ is used. To clarify the following, we adopt the following notations:

$$v_{Z;tot} = v_Z + v_Z^{\perp}; \tag{5}$$

with

$$v_Z = v_\perp + v_{\parallel Z} b; \tag{6}$$

$$v_Z^{\perp} = \frac{B \times \nabla p_Z}{Z n_Z e B^2}; \tag{7}$$

$$p_Z = n_Z T; \tag{8}$$

where T is the main plasma temperature ($T = T_e = T_i$), thus, impurities are assumed to be thermalized, n_Z is the impurity density, and $v_{\parallel Z}$ is given by an additional equation. Indeed, $v_{\parallel Z}$ cannot be equal to the plasma parallel velocity, otherwise the difference in the diamagnetic compressibility implied by $Z \neq 1$ and $p_Z \neq p$ would lead to large poloidal asymmetries. The $m=1$ component of the impurity parallel velocity thus relaxes to a value given by its own Pfirsch-Schlüter equilibrium, hence the need for an additional equation. Thus, the impurity velocity is the sum of the electric drift, common to all species, its own diamagnetic velocity and its own parallel velocity.

An *ad hoc* turbulent flux $\Gamma = -D_Z \nabla n_Z + n_Z v_{pZ}$ can be added, where D_Z is a diffusion coefficient and v_{pZ} is a pinch velocity, not necessarily constant radially. In this study, we made use of the pinch velocity only to benchmark the numerical model, but not for the impurity studies themselves, so we will remove it hereafter. In addition, a restoring source S_{n_Z} is added

$$S_{n_Z} = -\nabla \cdot (D_Z \nabla n_{Z0}); \tag{9}$$

where n_{Z0} is the initial impurity density profile.

Regarding the parallel velocity equation, we take the parallel component of the following impurity momentum equation, adopting the same assumptions as for the main plasma momentum equation:

$$q_Z (\partial_t v_Z + v_Z \cdot \nabla v_Z + v_Z^{\perp} \cdot \nabla v_\perp) = -\nabla p_Z + n_Z Z e (E + v_Z \times B) + R_Z; \tag{10}$$

where $q_Z = m_Z n_Z$, ($m_Z = A m_p$, where m_p is the proton mass), and R_Z is a dissipative force. In our study, we take the parallel component of R_Z to be a viscosity, implemented as a diffusion on $v_{\parallel Z}$ with a coefficient μ, which is the same as in the momentum equation, Eq. (2). This has the advantage that preconditioning of such diffusive terms is directly available and robust in XTOR-2F. Since we are in a regime where reconnection is dominated by the Hall term, that is, the parallel electron pressure gradient in Ohm's law, we take $E_{\parallel} = -\nabla_{\parallel} p_e / n_e e$. Note also that the parallel contribution of $\partial_t v_\perp$ is neglected.

Thus, the code solves the following set of coupled equations (in unnormalized form):

$$\partial_t n_Z = -\nabla \cdot (n_Z v_{Z;tot}) + \nabla \cdot D_Z \nabla (n_Z - n_{Z0}); \tag{11}$$

$$\partial_t v_{\parallel Z} = -\frac{1}{m_Z n_Z} v_Z \cdot \nabla v_Z + v_{\parallel Z} \cdot \nabla v_{\parallel Z} + \ldots - \frac{\nabla_{\parallel} p_Z}{m_Z n_Z} - Z \frac{\nabla_{\parallel} p_e}{m_Z n_e} + \nabla \cdot \mu \nabla v_{\parallel Z}; \tag{12}$$

Developing the total impurity velocity $v_{Z;tot}$, Eq. (11) can be recast into

$$\partial_t n_Z + v_\perp \cdot \nabla n_Z + v_{\parallel Z} \nabla_{\parallel} n_Z = \nabla \cdot D_Z \nabla (n_Z - n_{Z0}) \ldots - n_Z \left(\nabla \cdot v_\perp + v_{\parallel Z} b \right) + \frac{\nabla p_Z}{Z n_Z e} \cdot \nabla \times \frac{B}{B^2}; \tag{13}$$

The perpendicular velocity $v_\perp$, the electron density n_e, and the electron pressure $p_e = n_e T$ come from the resolution of the main plasma bifluid MHD equations. This form highlights the dominant mechanism, which is the advection by $v_\perp + v_{\parallel Z} b$ and the diffusion. The role of the second term on the r.h.s. is to restore particle conservation, and it also plays an important role during the nonlinear phase because of the generation of parallel velocity sheets. The equations are linear in n_Z and $v_{\parallel Z}$ so that normalization is not an issue. n_Z is normalized so that its values are of the order of 1. Also, notice the n_Z in the denominator in the two first terms of Eq. (12). Because of this term, the simulation diverges when n_Z vanishes. To avoid this scenario, we offset the profiles by a value of order unity, dictated by experience.

In this setup, the final impurity profile, after the sawtooth crash, depends mainly on the initial profile and diffusion coefficient, since the perpendicular flow is given by the main plasma evolution, which is fixed and is exactly the same throughout this study, and the impurity parallel velocity during the crash exhibits the same structure as that of the main plasma. Three kinds of initial profiles are presented in this study, to illustrate the effect of the crash on radial transport.

- Case 1: A very peaked profile, where all gradients are confined inside the initial $q=1$ surface. This unphysical configuration has a pedagogical interest since it helps to assess the quantities of impurities ejected by the sawtooth crash.
- Case 2: A hollow profile, flat inside the $q = 1$ surface and flat outside the $q=1$ surface, with a gradient in the region of the $q=1$ surface. Physically, this corresponds either to the case of an impurity with an outward pinch velocity creating a hollow profile or to a more complex scenario where an impurity, say, W, is generated at the boundary of the plasma, and slowly penetrates until it reaches the $q = 1$

surface. This can happen either at a W event[20] or during laser blow-off or supersonic beam injection experiments aiming at determining coefficient transport of impurities.[21,22] The simulation thus helps to determine how the sawtooth crash impacts the penetration of impurities. The offset value used in this case to prevent the impurity density from going to zero during the crash was 1, due to large gradients generated in this phase.

- Case 3: A peaked profile, designed as to mimic the Helium (He) ash produced by the fusion reactions. The fusion power P_{fus} is proportional to the square of the plasma density and to a certain power c of the temperature, $P_{fus} \propto n_e^2 T^c$, where $c(T)$ is close to 2 for typical fusion temperatures. In particular, $c(3.5\,\text{keV}) \approx 4.17$, $c(7.5\,\text{keV}) \approx 3$, and $c(26.6\,\text{keV}) \approx 1$. See Ref. 23 for the Deuterium-Tritium (D-T) fusion cross-sections and $\langle\sigma v\rangle$. Thus, it is a fair approximation to use $P_{fus} \propto p^2$ for a burning plasma, given that ITER volume average temperature should be around 13 keV, with peaks up to more than 25 keV.[24] Fig. 2 shows the pressure profile and the corresponding He source. The source is taken constant over time, even though pressure is modified by the sawtooth crashes. Also note that in the case of He, the hypothesis $T_Z = T$ does not hold since the α particles are generated with an energy of 3.5 MeV. However, the energetic particles are supposed to deposit their energy on the electrons before being removed from the plasma, so we can assume that at the sawtooth crash, the major part of the He content is thermalized. In other words, we assume the slowing down time of the α particles distribution is small compared to the transport time scales and the sawtooth period.

The pre-crash profiles for the three cases can be seen as the blue profiles of Figs. 9, 11(b), and 14.

For the charge and mass numbers of the impurities, we have taken $Z = 1$ and $A = 2$ for case 1, $Z = 2$, $A = 4$ for case 3 (helium), and different values for case 2, showing that it has little influence on the results.

The profile of the diffusion coefficient used in all three simulations is shown in Fig. 3. It increases by a factor of 10 between the core and the edge, with a transition located

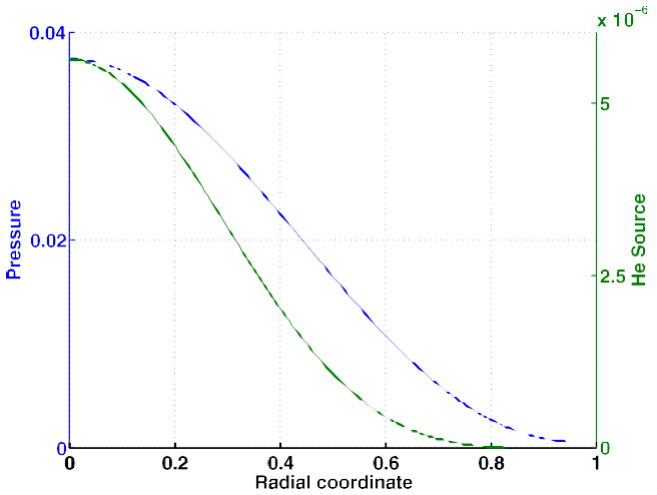

FIG. 2. Pressure profile in $q_0 V_A^2$ units (blue) and corresponding He source, normalized so that $n_{Z0}(0) - n_{Z0}(a) = 1$ (green) for case 3.

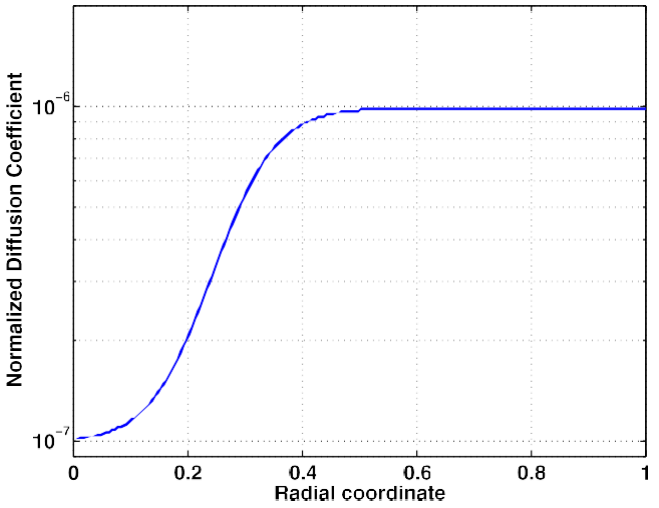

FIG. 3. Profiles of the diffusion coefficients used in the impurity simulations.

around the $q = 1$ surface. This mimics the experimental result that turbulence is much lower inside the $q = 1$ surface[25] and is also qualitatively consistent with critical gradient models, for instance, Ref. 26. The absolute value in the core is taken to be of the same order of magnitude as the measured diffusion coefficient for the electron density. Notice that in this study, we are mainly interested in the transport induced by the sawtooth crash, which is sufficiently fast so that the detail of the transport coefficients does not matter much.

In cases 1 and 2, the impurity density is given analytically and the source determined from Eq. (9). In case 3, the direct implementation of $S_{n_Z} \propto p^2$, with p constant on flux surfaces, leads to poloidal asymmetries due to the equilibrium metric, thereby making interpretation harder. Therefore, the density n_{Z0} is determined by a 1D diffusion code assuming circular and concentric flux surfaces. The density obtained by this means, constant on flux surfaces, is plugged into XTOR-2F and once again the source is determined from Eq. (9).

We now present a benchmark of the impurity model. To check the model, we simulate an impurity which has the same initial profile, mass and charge numbers, and transport coefficients as the plasma density. Thus, the density equations are the same, and the only difference is the expression for the parallel velocity because of the viscosity term.

The density profile before the sawtooth crash is chosen arbitrarily. It exhibits a drop of 15% between the core and the $q = 1$ surface. The results are also compared with a pure advection simulation, that is, a simulation in which the density verifies the following equation:

$$\partial_t n_Z + \mathbf{v} \cdot \nabla n_Z = \nabla \cdot (D_Z \nabla (n_Z - n_{Z0})); \qquad (14)$$

where $\mathbf{v} = \mathbf{v}_\parallel + \mathbf{v}_{\parallel\parallel}$ is the plasma velocity, given by the resolution of Eqs. (1)–(4). The results are shown in Fig. 4, where the initial and post-crash flux-surface averaged profiles are compared for the different cases. The black curve is the initial density, the blue curve is the post-crash density coming from the full resolution, the red dashed curve is its

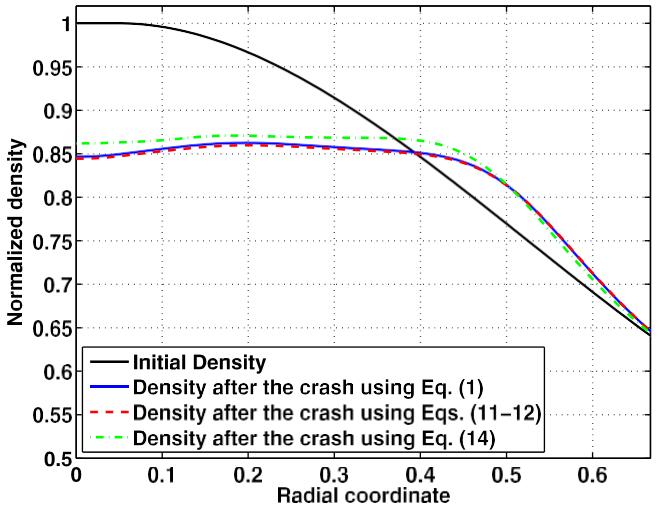

FIG. 4. Comparison of the flux surface average of the density towards the end of the reconnection phase, obtained with Eq. (1) (blue), with Eqs. (11) and (12) (red-dash) and with Eq. (14) (green dot-dash). The pre-crash density profile is shown as the black curve.

reproduction using Eqs. (11) and (12) and the green dotted-dashed curve uses only advection, Eq. (14). As expected, the blue and red-dashed curves agree very well, within 0.5%. The small remaining difference can be attributed to the difference in the implementation of viscosity. However, there is a 1%–2% difference in the core between the green curve and the blue curve, showing that pure advection is unable to capture all the physics of density redistribution by the sawtooth crash. Indeed, although the difference may seem small, we want to look at potentially small structures and effects, which seem to be captured only by the bifluid model.

An additional confirmation of the need of Eqs. (11) and (12) for our study is provided by an other simulation, where the initial profile is the same as in Ref. 12. The profile is less peaked and the post-crash profile is very sensitive to the model used, as can be seen in Fig. 5. In this case, pure advection completely fails to reproduce the post-crash structures.

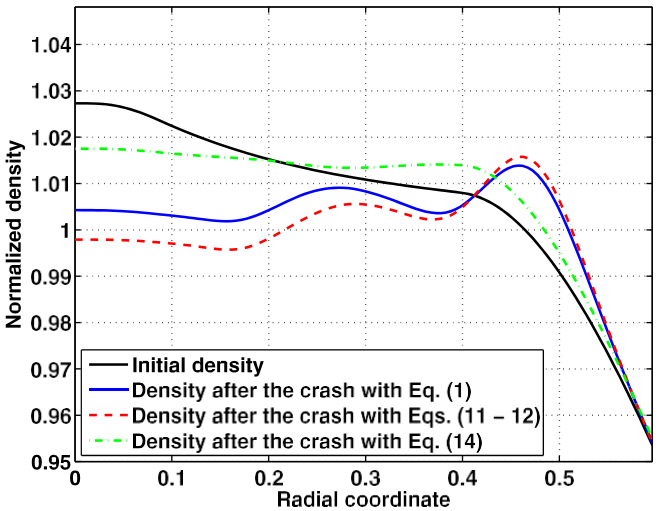

FIG. 5. Comparison of the flux surface average of the density towards the end of the reconnection phase, obtained with Eq. (1) (blue), with Eqs. (11) and (12) (red-dash), and with Eq. (14) (green dot-dash). The pre-crash density profile is shown as the black curve; it is the same as in Ref. 12.

In particular, the benchmark helps to highlight the physics involved in the generation of the post-crash crescent-shaped structure detailed in Ref. 12. The poloidal color plots of the density corresponding to Fig. 5 are shown in Fig. 6. Fig. 6(a) corresponds to the red dashed curve of Figs. 5 and 6(b) corresponds to the green dotted-dashed curve of Fig. 5. The first simulation clearly exhibits a crescent-shaped structure well inside the q¼1 surface, while the second one does not display any crescent structure, showing that the physics of compressibility and in particular parallel compressibility is crucial to obtain this structure.

In the following impurity study, we will keep in mind that the crescent-shaped structure of Fig. 6(a) raises the question of the particle redistribution and seems to indicate that a significant part of the core density is reinjected inside the q¼1 surface. On the electron density, this is not a concern since it represents a very small amount of the total density. The concern is that with more peaked profiles, like He, for instance, which is produced in the core, the effect could be enhanced and lead to a higher He concentration on average.

IV. RESULTS

A. Case 1

We now proceed with the analysis of case 1. To assess the quantity of impurity that leaves the q ¼ 1 surface, we compute the quantity N_{Z1} ðtÞ defined by the following integral:

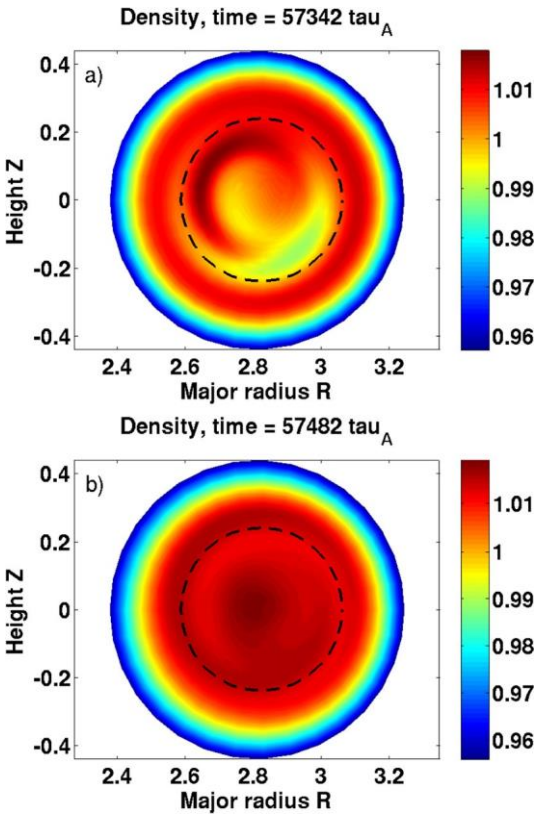

FIG. 6. Comparison between two simulations of electron density using the impurity model, one with a separate impurity parallel velocity equation (a), and one with pure advection (b).

$$N_{Z1}(t) = \int_{V_{q=1}} [n_Z(r, t) - n_Z(r = r_s, 0)]\, d^3r; \qquad (15)$$

where $V_{q=1}$ is the volume bounded by the magnetic axis and the flux surface located at $r = r_s$, the radius of the $q = 1$ surface. We express it in percentage of the initial value, $N_{Z1}\%(t) = 100 N_{Z1}(t)/N_{Z1}(0)$ where $t = 0$ refers to the beginning of the pressure drop corresponding to the shift of the core due to the internal kink mode. Fig. 7 shows the evolution of the quantity $N_{Z1}\%$ during a sawtooth crash. The reference time is the time at which the curve starts to decrease.

It is seen that the curve goes to a minimum of around 20% at the end of the reconnection phase. There is a small fast rise of approximately 5% before diffusive evolution (diffusion and source) takes over to rebuild the profile until the next sawtooth crash. The 5% rise at the end of the reconnection phase is due to the small remaining flows necessary to restore the initial topology of the flux surfaces. Indeed, in Fig. 8, a Poincaré plot of the magnetic surfaces taken at the time of the rise, it can be seen that when the core has been completely reconnected, the new core has not stabilized yet. Following the principle that when ideal MHD is valid (which should be the case in the newly formed core) the frozen-in-law is valid, a displacement of the magnetic surfaces also implies a displacement of the plasma, and some reorganization of the impurity density occurs at this time.

Nevertheless, we can see that the amount of particles inside the $q = 1$ surface after the crash is small, globally the sawtooth efficiently flushed the impurities away from the core. Fig. 9 shows some flux surface averaged profiles during the reconnection phase. The reference time is the same as in Fig. 7. The formation of a "hump" at a location close to the mixing radius (see Sec. V) is clearly visible. This happens because the density is mainly advected by the flows, which are dominantly located at the reconnection separatrix. This separatrix moves from the initial $q = 1$ surface until the mixing radius at the end of the reconnection phase, and the density follows.

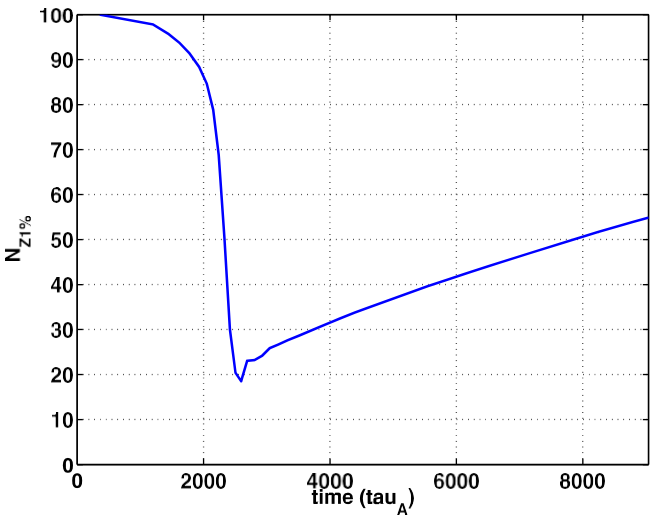

FIG. 7. Evolution of $N_{Z1}\%$ during a sawtooth crash for case 1.

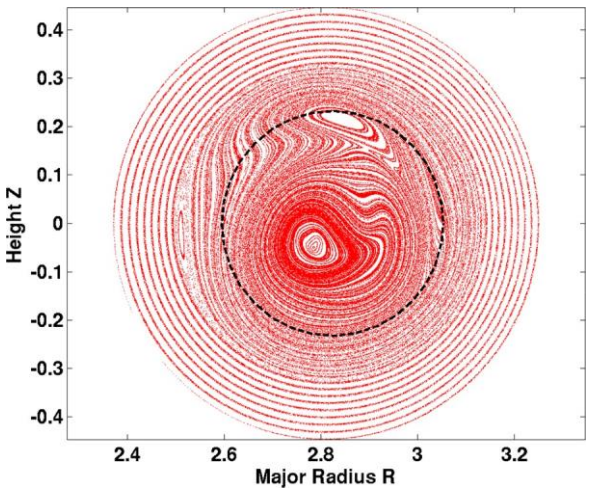

FIG. 8. Poincare plot at the end of the reconnection phase. The small remainder of the reconnecting core can be observed at the left of the figure, well beyond the initial $q = 1$ surface location (dashed circle), at a location corresponding to the mixing radius.

No post-crash crescent-shaped structure can be observed in this case, as seen in Fig. 10. It does not seem to be due to some physics missing in the model since the same model obtains crescent with the profiles of Fig. 5. So it seems to indicate that the crescent structure is dependent on the details of the pre-crash profiles.

B. Case 2

We now come to case 2. Following the methodology of case 1, we compute a quantity $N_{Z2}\%(t)$, where now it is defined by

$$N_{Z2}\%(t) = \frac{100}{A} \int_{V_{core}} [n_Z(r, t) - n_Z(r, 0)]\, d^3r; \qquad (16)$$

where now V_{core} is bounded by the magnetic axis and the radius where the equilibrium impurity density starts to increase, $s = 0.3$ ($s = \frac{r}{w}\frac{dw}{dr}\big|_{w=w_a}$). $N_0 = 1$ is the offset value,

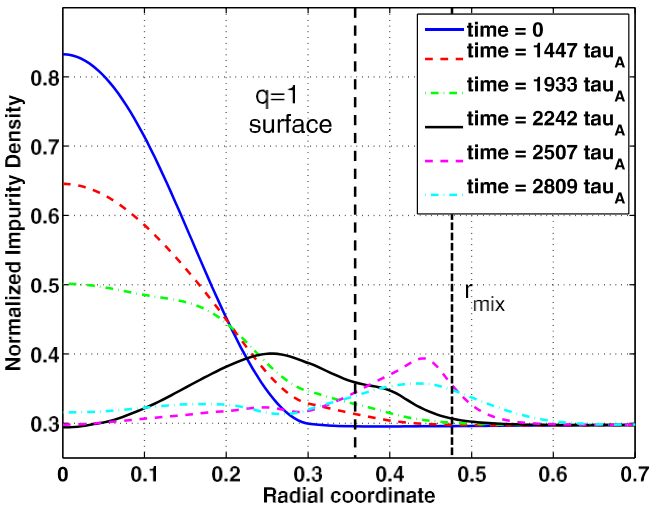

FIG. 9. Flux surface averaged impurity density profiles before, during and after the sawtooth crash for case 1. The initial $q = 1$ surface and mixing radius are represented by the vertical dashed lines.

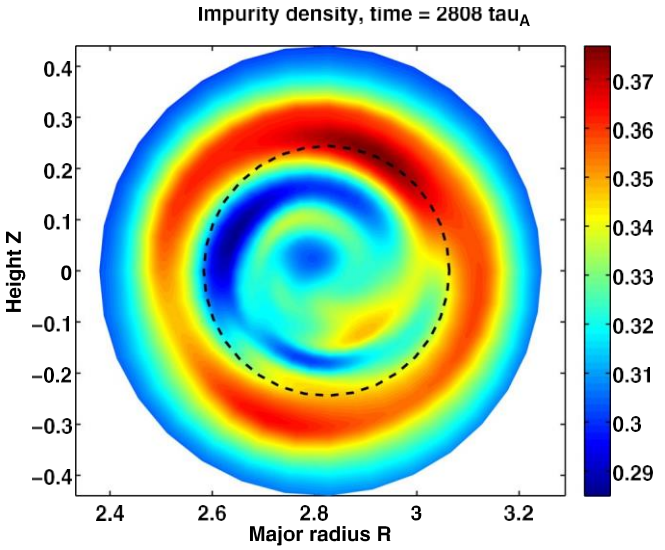

FIG. 10. Post-crash poloidal density profile obtained in case 1. The dashed circle is the position of the pre-crash $q=1$ surface. There is no trace of a crescent-shaped structure.

and A is a normalization constant, such that $A = \int_{V_{core}} d^3r$, so that $N_{Z2}\% = 100\%$ when the core impurity density is equal to the external density everywhere. The results are presented in Fig. 11. The same kind of behaviour can be observed as in case 1, but inverted. Now the crash leads to a penetration of impurities, indeed the flows connect the external region to the internal region. At the beginning, the penetration is very important, and we observe a spiky behaviour, similar to case 1 but much more pronounced. $N_{Z2}\%$ reaches 50% transiently, then falls rapidly to 30%, and finally decreases diffusively until the following crash. The relevant profile to look at is the profile at the end of the spike phase, the magenta profile in Fig. 11(b), with an impurity density approximately flat and equal to 1.3 in the core, compared to 1 initially and 2 in the external region. Thus, our simulations indicate that the sawtooth crash efficiently leads to the penetration of impurities up to the magnetic axis. This has been experimentally observed during impurity injection experiments on the JET[27] and ASDEX Upgrade[3] tokamaks. This is quite preoccupying because this means that when W is generated at the walls and enters the plasma, if it has an inward pinch velocity and reaches the $q=1$ surface, it will be rapidly, in a reconnection time, driven to the very core of the tokamak. This can lead to a radiative collapse because the core of a burning fusion plasma is much hotter than the $q = 1$ surface, and a given W concentration can be tolerable at the $q = 1$ surface but intolerable in the hot core.

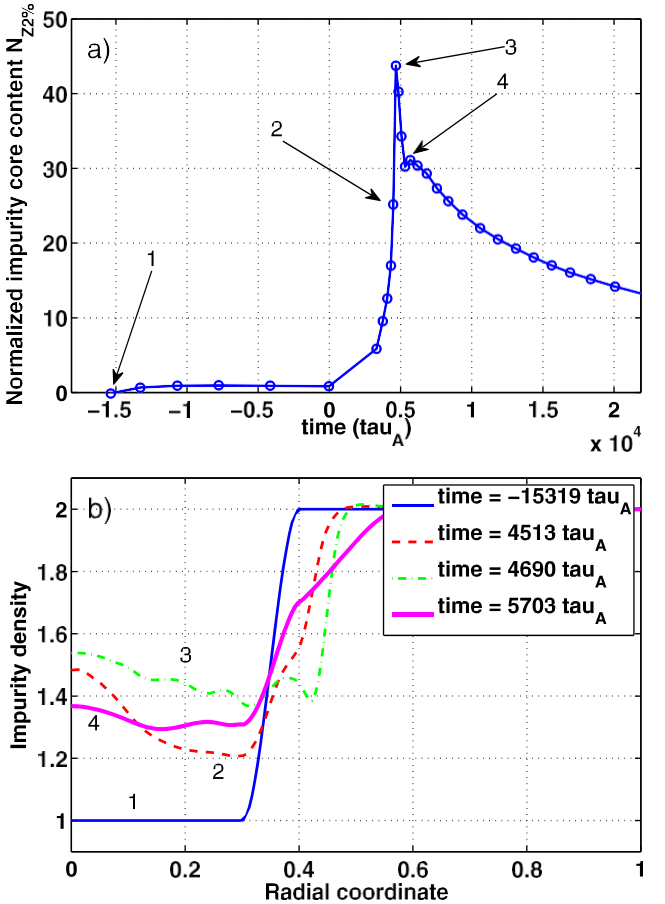

FIG. 11. Evolution of $N_{Z2}\%$ during a sawtooth crash (a) and impurity core density profiles (b) for case 2. The numbers in the profiles correspond to the numbers indicating the times in panel (a).

We now discuss the influence of the parameters Z and A which characterize the impurity species. The charge Z is taken into account in our model in order to model properly the diamagnetic velocity of the impurity, implying the resolution of an additional parallel velocity equation. Obviously, the parameter A, which represents the inertia of the impurities, affects the dynamics of the impurity parallel velocity. During the sawtooth crash, when parallel gradients significantly depart from zero, the two first terms on the r.h.s. of Eq. (12) will lead to parallel acceleration. The first scales as $1/A$ and thus will be small for heavy impurities. The second one scales as Z/A and can remain large even for heavy impurities, providing the plasma is hot enough for the impurity to be fully stripped. Nonetheless, we see that the basic physics is not modified when varying A and Z. The only difference will be the relative amplitude of the parallel velocity sheets generated in the vicinity of the $q=1$ surface, but the dominant effect on the particles during the crash remains the advection by the perpendicular flows,[12] so that we do not expect a significant difference on the results for the impurity density. Notice that for this study, we dropped the inertia terms $\delta v_Z \cdot \nabla v_Z + v_Z^2 \cdot \nabla v_{\parallel}|_{jj}$. It was not expected to play any significant role for the comparison at different values of A and Z and we could check at moderate A and Z that indeed it does not modify the results.

For the benchmark, we have used 4 couples $(A; Z)$. First the value used throughout this article, $(A; Z) = (2; 1)$, which is the deuterium value. Then multiplying both by ten, and again by two, the values (20,10) and (40,20) are used, keeping the ratio $A/Z = 2$. Finally, a value which is relevant to W has been used, $(A; Z) = (184; 40)$. The mass number of W is 183.84 and $Z=40$ is a typical order of magnitude for W at temperatures of a few keV (see Figure 6 of Ref. 28). The results are presented in Fig. 12. It is seen that there are virtually no quantitative differences between the four cases, as expected. This shows that the mass and charge numbers of the impurities have very little influence on their dynamics

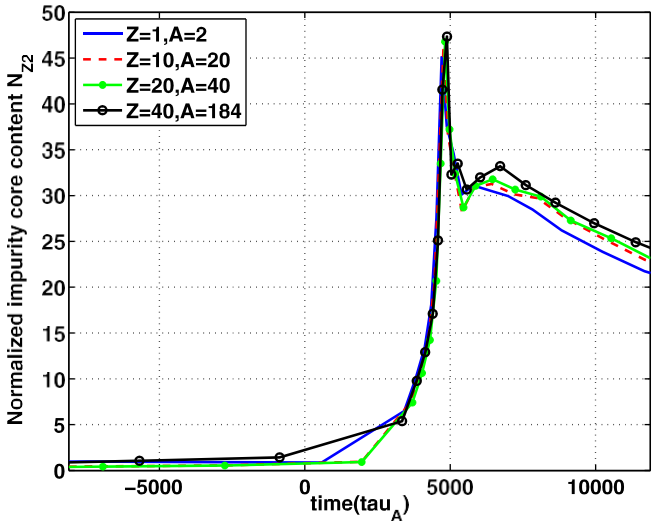

FIG. 12. Comparison between different values of A and Z for a hollow profile.

during the crash. This is of course, however, not true at all during the quiescent MHD free evolution of the plasma, where strong dependence of the neoclassical and turbulent transport coefficients are found theoretically and numerically, and observed experimentally.[29–31]

C. Case 3

We now present the results for case 3. Recall that this corresponds to a He source from fusion reactions. The reader should keep in mind that what matters is the long term average He density profile in the core. If it is too large and there is no efficient way to extract the Helium ash after it has delivered its heat to the plasma, it may stifle the fusion reactions by diluting the D-T mix. For instance, for a 500 MW machine like ITER, a sawtooth period s_{ST} larger than 10 s, as predicted by Ref. 32, leads to a He buildup comparable to the density of the mixture, which starts reducing the fusion power. Indeed, considering that $\langle \sigma v \rangle_{DT} > 10^{-21}$ m^3.s^{-1} for $T_i > 10$ keV,[23] and with Deuterium and Tritium densities $n_D \sim n_T \sim 10^{20}$ m^{-3}, the ratio R between the He density resulting from the fusion reactions between two sawtooth crashes (assuming no transport) and the Deuterium density, $R = n_D n_T \langle \sigma v \rangle s_{ST} / n_D = n_T \langle \sigma v \rangle s_{ST}$, can easily reach unity, which leads to a decrease of the D-T mixture density unless the α particles are adequately evacuated and D-T efficiently replaced in the core. Thus, if the sawtooth crash does not flush the core efficiently enough, the impurity content can be increased, leading to dilution for the case of He ash and possibly to radiative collapse in the case of W.

Obviously, the average impurity content of the core will be highly dependent on the sawtooth period s_{ST} or more precisely to the ratio between s_{ST} and the diffusive time $a^2/D_{Z?}$. s_{ST} is fixed by our equilibrium and our choice of S and α, and $D_{Z?}$ can be quite easily modified. However, an extensive numerical study would have required an excessive amount of computational time, hence, we did only two simulations, one with the diffusion of Fig. 3 and one with the same profile scaled up by a factor of three. We will focus on the first case, with the profile of Fig. 3, and it will be seen that the other case confirms the results. Even though we will compute an average impurity density over a sawtooth cycle after reaching stationarity, we will not discuss in detail this mere result directly, but rather we will focus on the comparison with the 1D model derived from Kadomtsev rules in Sec. V.

Fig. 13 shows the pre-crash and post-crash 2D poloidal He profiles for case 3. The corresponding flux surface averaged profiles are represented in Fig. 14. It is seen how the impurity density has been dominantly remapped on a ring located outside the $q=1$ surface. This location corresponds to the mixing radius. Hence, the phenomenology is the same as in case 1. This time, we see a crescent-shaped structure; its amplitude is about 3% of the impurity density. It is much smaller than the external ring, which has an amplitude of about 8%. Compared to the total impurity content inside the $q=1$ surface (in excess of the density at $q=1$, see Eq. (15)), the amount of particles contained in the small crescent is slightly less than 10%. Thus, it seems rather unimportant and not a source of concern regarding the impurity flushing during the sawtooth crash. We do not develop further the analysis, which is mainly done in the Sec. V, together with the comparison to a 1D redistribution model.

V. COMPARISON WITH A 1-D KADOMTSEV MODEL

Conventional wisdom assumes density and temperature profiles to be flat after a sawtooth crash, from the magnetic

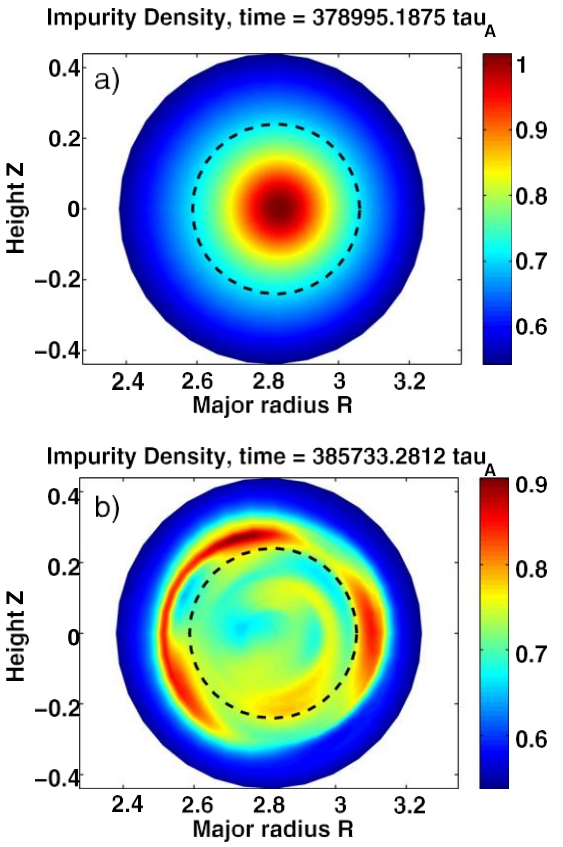

FIG. 13. Surface plots of the pre-crash (a) and post-crash (b) 2D density profiles in the poloidal plane for case 3 (He-like). The dashed circle represents the initial $q=1$ surface.

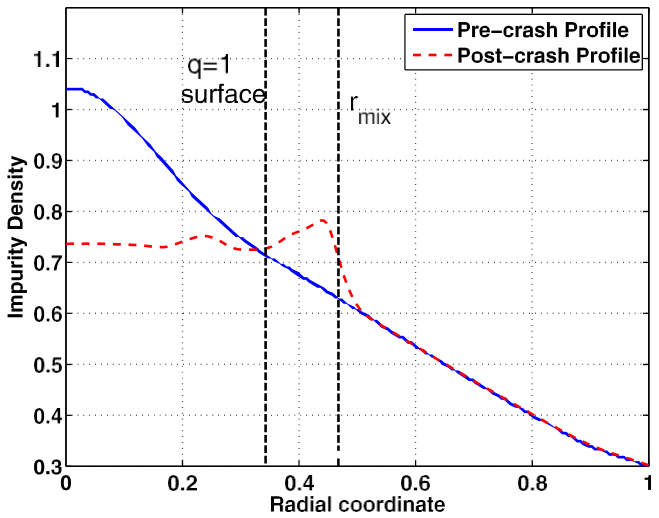

FIG. 14. Flux surface averaged profiles corresponding to Fig. 13.

axis up to the mixing radius r_{mix}. See for instance, Ref. 32, where this assumption is repeatedly made. Hereafter, we derive a simple rule to transform 1D profiles under the action of a sawtooth crash, based on Kadomtsev complete reconnection assumption, and show that profiles are not flat but often display a hump between the $q=1$ surface and the mixing radius. This is not new, although this may not be well known. The model is a simpler version of the model used in Refs. 16 and 17. In these contributions, in addition to conservation rules, a heat source and a diffusion during the crash are added, and the poloidal island structure is given by an analytical expression depending on the MHD displacement, which is given by the experiment. Here, we suppose the sources and diffusion to be too slow to matter during the sawtooth crash. This allows to work on 1D profiles rather than 2D or 3D profiles. Hence, in the following, we will denote the model simply as Kadomtsev's model. It is based on the following assumptions.

- Conservation of the helical flux $W^?$. Surfaces with same helical flux reconnect and are deformed until they take the form of a (convex) torus around the newly formed magnetic axis.
- Conservation of the toroidal flux W_T. The final flux surface obtained from the two reconnecting surfaces has the same toroidal flux as the difference between the toroidal fluxes of the reconnecting surfaces.
- Conservation of energy and particles. Energy conservation allows to compute the final pressure, while particle conservation allows to compute the final density profile.

The helical flux is the magnetic flux through an $(\theta; n)=(1;)$ ribbon. It can be expressed as a function of the safety factor q

$$W^?(w_0) = \int_0^{w_0} (1 - q(w))\,dw; \qquad (17)$$

where w_0 is the initial poloidal flux, such that dW_T/dw_0. Since surfaces with identical helical flux reconnect, the magnetic surface, which is the last one to reconnect, matches the surface which has $W^? = 0$. Thus, reconnection affects the plasma up to a radius called mixing radius r_{mix}, such that $W^?(r_{mix}) = 0$. For monotonic q profile, and $q(0) < 1$, the helical flux has a vanishing radial derivative in $r = 0$ and $r = r_s$, it increases from $r = 0$ to $r = r_s$ and then decreases up to 0 at r_{mix}. Fig. 15 shows the helical flux obtained with the pre-crash safety factor in our XTOR-2F simulations. Note that this safety factor in the stationary sawtooth regime is not equal to the initial, equilibrium one. Indeed, between two crashes, the safety factor evolves resistively until the next sawtooth crash is triggered, which happens before it has reached its initial value.

In the following, we call radius and denote by r the radial coordinate in XTOR-2F, which is equal to the square root of the initial normalized poloidal flux.

In practice, the helical flux is computed, its maximum value $W^?_{max}$ is determined, and the interval $[0; W^?_{max}]$ is sampled with n_W values. For each value $W^?$ of the helical flux, the radii of the reconnecting surfaces on the left and the right of the separatrix, $r_l(W^?)$ and $r_r(W^?)$, are determined, and the toroidal flux increments between the new radii and the ones obtained at the preceding step are computed on the left and on the right: $dW_{T;l}(W^?)$ and $dW_{T;r}(W^?)$. The final radius $r_f(W^?)$ of the surface with helical flux $W^?$ is determined from the condition of toroidal flux conservation

$$W_{T;f}(W^?) = \int_{W=0}^{W^?} dW_{T;l}(W) + dW_{T;r}(W) \; ; \qquad (18)$$

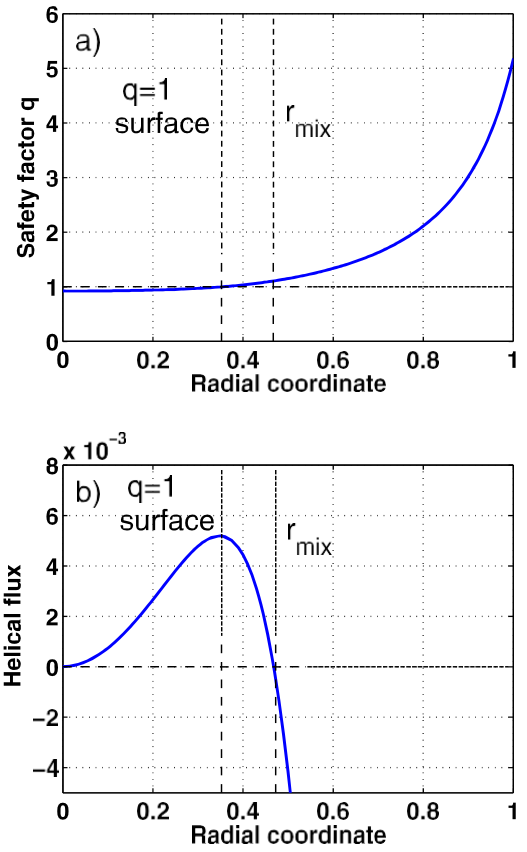

FIG. 15. Pre-crash safety factor profile (a) and corresponding helical flux (b) in the XTOR-2F simulations. The central value of the safety factor is $q_0 = 0.93$.

and the correspondence between radius and toroidal flux is used.

The final density or pressure, generically denoted n_f, is determined as a function of the initial profile n_i, according to the conservation rule, and using the fact that toroidal flux conservation is almost the same as volume conservation. Thus, we find

$$n_f(r_f(\Psi)) = \frac{n_i(r_l(\Psi))\,d\Psi_{T;l}(\Psi) + n_i(r_r(\Psi))\,d\Psi_{T;r}(\Psi)}{d\Psi_{T;l}(\Psi) + d\Psi_{T;r}(\Psi)}. \quad (19)$$

There are special cases where the final profile using this method is flat. For example, for circular concentric flux surfaces labeled by the minor radius a, a q profile of the form

$$q = \frac{q_0}{1-(1-q_0)\left(\frac{r}{r_s}\right)^2}; \quad (20)$$

and parabolic pressure and density profiles, the final profiles can be computed analytically for circular concentric flux surfaces, and they are rigorously flat.[16] However, in the general case, it is not true.

To compare the redistribution model with the results of XTOR-2F, we used the code in an MHD stable situation with exactly the same source and diffusion for the impurity, and we applied the profile redistribution described above every time there is a sawtooth crash. To obtain a stable MHD equilibrium, we raised the q profile above unity in the core. This modifies the equilibrium, however, the operation is done without modifying the metrics, so that in both cases the source computed from $-\nabla\cdot D_Z\,\nabla n_Z$ is identical and the comparison meaningful. The safety factor profile used in the redistribution model is the profile taken from the full XTOR-2F simulation, just before the sawtooth crash is triggered.

Fig. 16 shows the initial and post-crash profiles corresponding to case 3, obtained with this model (black) and with the full non-linear bifluid MHD code (red) after a typical crash. The profiles are very similar. They both present a hump close to r_{mix} and the core values are similar. In the case of Kadomtsev's model, it is even a spike with a sharp discontinuity at r_{mix}. The origin of this spike is that the toroidal (or volume) increments on both sides of the separatrix tend to have very similar values, hence the final density is merely the mean of the density in $r_l(\Psi)$ and $r_r(\Psi)$. The final density on the new magnetic axis is equal to $n_i(r_s)$ while the density at r_{mix} is the mean between the initial density on the magnetic axis and the initial density at r_{mix}. Since r_{mix} is close to r_s, we obtain that the final density at the mixing radius is of the order of $(n_i(r_s) + n_i(0))/2 > n_i(r_s)$.

The XTOR-2F profile has also a sharp transition to the external unaffected profile centered around r_{mix}. It is striking that the model derived from mere transport along the field lines agrees well with the XTOR-2F results, despite completely different mechanisms. In the XTOR-2F case, the particle transport is due to advection by the kink and reconnection flows, which overall have a double convection cell structure. Since kinetic energy is located dominantly behind the reconnection site, that is, on the separatrix, density accumulates there and leads to the formation of the observed hump. At the end of the reconnection, the separatrix is at r_{mix}, hence the agreement between Kadomtsev's model and XTOR-2F results in Fig. 16.

Fig. 17 shows the central impurity density for both models. It is seen that the bottom value after the crash is well predicted by Kadomtsev's model. This is the value of the density at the initial $q=1$ surface. The top value is higher in Kadomtsev's model case. This is because the crash is instantaneous in the model, whereas it actually takes a few thousands s_A for the flux to reconnect in XTOR-2F. Thus, when the core is initially displaced by the kink, the core value starts to drop, while in Kadomtsev's model it continues to rise diffusively until the crash is triggered. Overall the profiles are very close in the evolution, which is not surprising since in between crashes, the evolution is dominated by diffusion, which is identical in both cases. A last comparison is

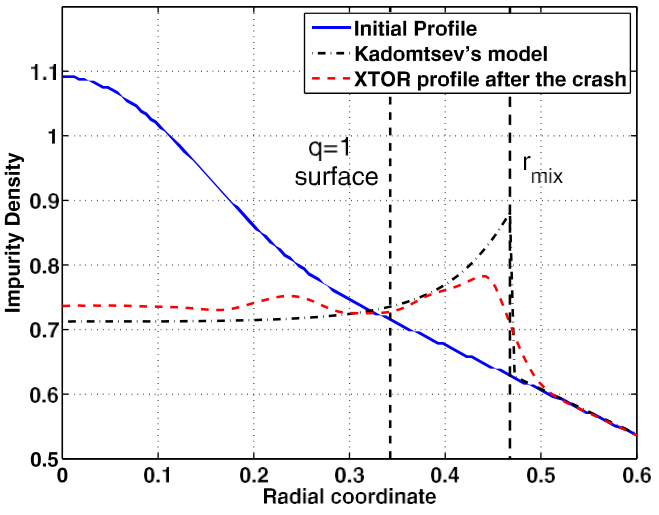

FIG. 16. Initial (blue) and post-crash (green dash-dot) profile for the peaked He profile of Sec. IV, case 3. The red dashed curve shows the post-crash profile given by XTOR-2F.

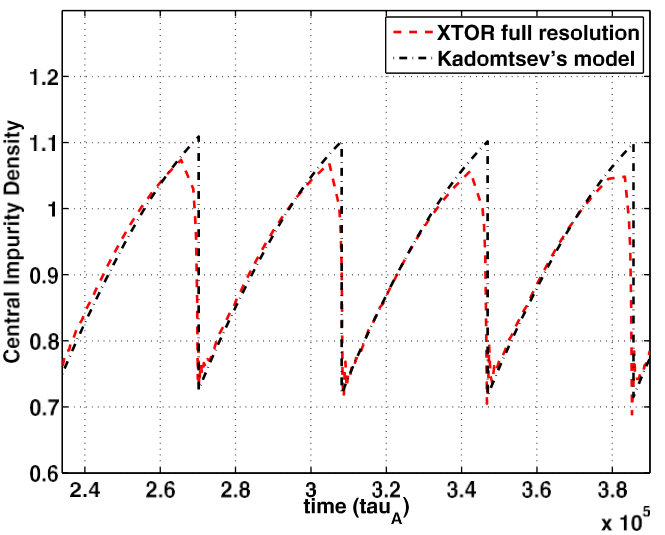

FIG. 17. Central impurity density in the XTOR-2F case (red) and with Kadomtsev's model (green).

obtained by plotting the time-averaged profile over a sawtooth cycle. The result is shown in Fig. 18(a), where the agreement is observed once again. Fig. 18(b) shows the same analysis for the case with the increased diffusion coefficient, which clearly confirms the results. As expected, the central value in Kadomtsev's model case is slightly higher because the crash is instantaneous and thus triggered a bit later. However, the overall agreement is good, within 2%. The profile at the maximum of the ramp is also plotted in blue.

It is also interesting to perform the comparison on the hollow profile. The results can be seen in Fig. 19. The redistributed profile is very similar to the XTOR-2F profile obtained at the top of the spike in Fig. 11(a), as shown with the red profile. However, it has been mentioned that the remaining flows at the end of the reconnection phase reduce the value of the impurity content obtained at the top of the spike down to a smaller value. The relevant profile is the magenta profile of Fig. 11 (number 4), reported in Fig. 11 as well. Thus, the Kadomtsev's model slightly overestimates the impurity penetration.

VI. DISCUSSION

Going back to the motivation in the Introduction, it appears that the detail of the pre-crash peaking matters for the formation of the crescent-shaped structure, which is the result of a complex interaction between the initial gradients, the advecting flows and the compressibility. When they are visible, their amplitude is small and they should finally not be considered as a source of concern regarding the sawtooth flushing mechanism. Notice that contrary to the electron density results, these results cannot be easily compared to the experiment, because impurity density measurements are not available yet with sufficient precision. Only density estimates and rough structures can be inferred from soft X-ray tomography and spectroscopic measurements coupled to temperature and electron density measurements.[2,28,33]

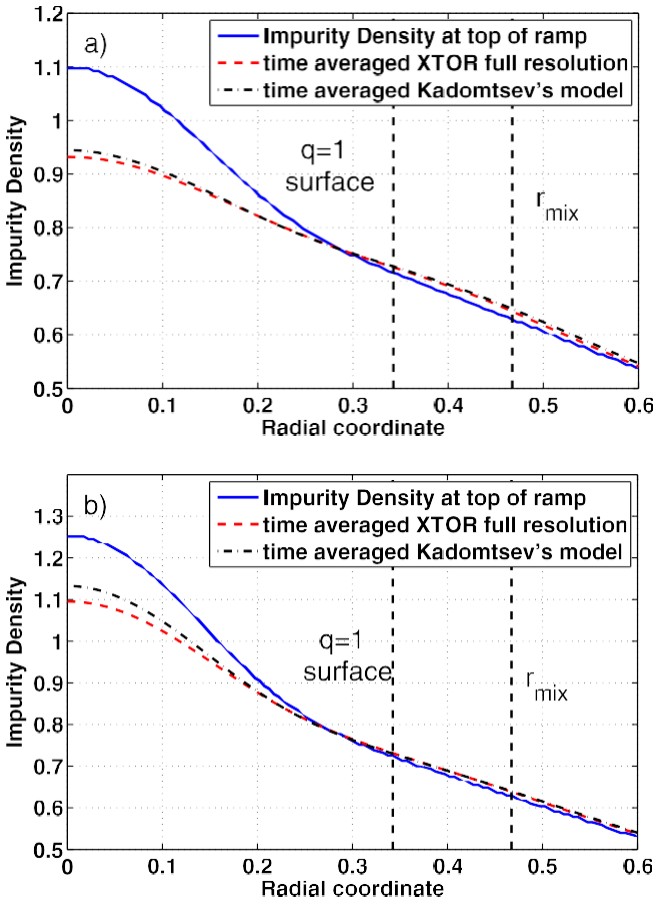

FIG. 18. Time-averaged density for the XTOR-2F case (red) and Kadomtsev's model case (green). In blue, the impurity density at the maximum of a sawtooth ramp is plotted (a). Same figure in (b) for a diffusion coefficient scaled up by a factor of three.

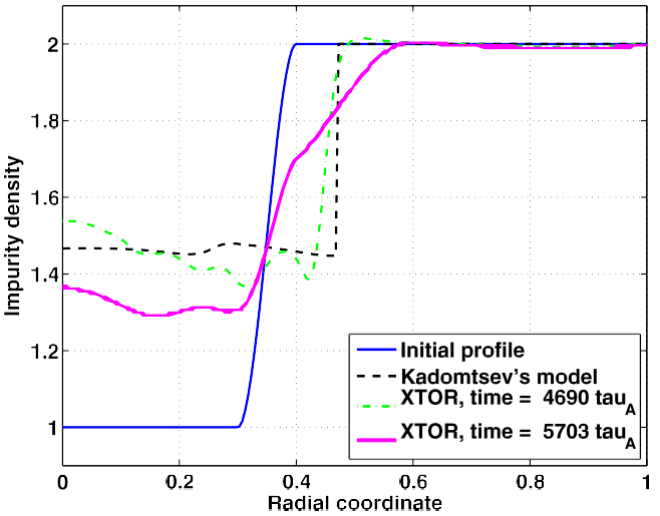

FIG. 19. Comparison between XTOR-2F and Kadomtsev's model for the hollow case (case 2).

The main *caveat* of this study is the full reconnection observed in XTOR-2F. Indeed, most experimental evidence point to the relevance of incomplete reconnection in most cases. Up to now, no self-consistent MHD model has been able to simulate sawteeth with incomplete reconnection, to the authors' knowledge. Hence, we chose to use full reconnection also with Kadomtsev's model. This constraint on the model could be easily released, and the reader can refer to Refs. 16 and 32 for an interesting example. However, the agreement between such models and full MHD models like XTOR-2F cannot be guaranteed in the case of incomplete reconnection. It would be ideal to possess an MHD code able to simulate incomplete reconnection, in the vein of Ref. 34 for instance, together with self-consistent sawteeth, but this is currently not available.

The agreement between XTOR-2F and Kadomtsev's model seems unexpected because of the inherently different redistribution mechanisms, however, as mentioned above, basically we expect both models to yield similar core values after the crash ($n_{Z0}(r_s)$), and to display a hump around r_{mix}, in the one case because of pure volume element matters, in the XTOR-2F case because the flow is most important on the separatrix, which ends on r_{mix} at the end of the reconnection phase. Nevertheless, Kadomtsev's model overestimates the penetration in the hollow case.

We have not focused a lot on the mere values obtained in these simulations, because, as mentioned above, they depend on the ratio between diffusive time and sawtooth

period. In our simulations, this ratio assumes quite frequent sawteeth, more or less in the range of Tore Supra ohmic sawteeth with periods of the order of 30 ms. We have taken $D_Z s_{ST}/a^2 \sim 4 \times 10^{-3}$, which is consistent with a core particle diffusivity of 5×10^{-2} m^2 s^{-1} (measured value for electrons in the core[25]), a sawtooth period of 30 ms and a plasma radius $a \approx 0.7$ m. In reactors, the sawtooth period is expected to be much longer, of the order of several seconds, or tens of seconds,[32] reducing by much the usefulness of sawteeth as a means to expel impurities or He ash from the core of the tokamak. This could, however, be changed if sawtooth control is used on ITER, following the strategy presented in Refs. 35 and 36, for example.

We would also like to point out that Kadomtsev's model is of use only if a convincing triggering threshold is known for the sawtooth crash. There have been several attempts to derive a criterion for sawtooth triggering, or, equivalently, a prediction for the sawtooth period.[32,37] The subject is still debated, but such semi-heuristic models are usually in reasonable agreement with the experiments. At the least, if one wants to simulate the sawtooth induced transport for a real experimental discharge, it is possible to take the experimentally measured sawtooth period.

Considering that the agreement between our nonlinear electron density MHD simulations and the experiment presented in Ref. 12 was only qualitative, there may still be some physics missing in XTOR-2F to explain the crescent-shaped structure. Regarding this point, some authors proposed[38,39] that the sawtooth crash happens in two phases, the first, Kadomtsev-like, relaxes the q profile to 1, and the second, due to the remaining kinetic energy accumulated in the core due to the reconnection jets, reconnects the helical flux in a Wesson-like[40] process, leading to $q < 1$. The mechanism invoked and numerically demonstrated in Ref. 39 is the electron inertia combined with hyperresistivity and flow damping. This Wesson mechanism clearly involves reinjection in the core of a part of the primarily reconnected flux. While it should not affect the temperature, which is usually flattened by Kadomtsev reconnection, this may indeed be a mechanism able to reinject particles from the external denser ring observed on the impurity density (notice that Kadomtsev reconnection flattening the profiles or not depends only on the detail of the pre-crash profile). Electron inertia is not present in the code and we do not observe any Wesson-like second phase. However, the observation of the spike in Fig. 11(a), which implies a modification of the core particle content after the end of the reconnection phase, was attributed to the flows remaining after the crash. There may be a link with the physics described in this paragraph. The introduction of electron inertia in full MHD sawtooth crash simulations would be very instructive in this regard.

As a final remark, notice that a few instances of crescent-shaped structures can be found in the literature, in particular in JET[41] and TFTR,[42] observed using soft X-ray tomography in both cases. We believe these structures are distinct from the one we investigate in the present study. In the JET case, the crescent is observed during the reconnection phase and is attributed to a possible Wesson-like process. In TFTR, the structure is attributed to a relic of the old core which is diffused on time scales longer than the sawtooth crash. Instead, the crescent structure we have discussed here was initially observed directly on the electron density after the sawtooth crash and results from the complex dynamics of Kadomtsev-like reconnection flows.

VII. CONCLUSION

We can summarize the results of this work in four main points

1. The crescent-shaped structures can be observed on the post-crash profiles for some impurity density profiles, although they do not seem to be a universal feature of the post-crash profiles simulated by XTOR-2F's MHD model. In any case, their amplitude is small and should not be regarded as a source of concern for impurity redistribution by the sawtooth crash.
2. Peaked profiles tend to produce large humps at the location of r_{mix}, because the separatrix where the flows are located moves from the $q=1$ surface up to r_{mix}. The flow drives the dense core toward the separatrix and maps it to an external ring which ends up close to r_{mix}.
3. In the case of hollow profiles, there is a significant penetration of the impurities up to the magnetic axis. This has been experimentally seen on the JET tokamak and may be a serious issue for Tungsten operation.
4. A 1D model based on Kadomtsev's principles is seen to reproduce the XTOR-2F results with a fairly good agreement in the case of peaked profiles. However, it overestimates the impurity penetration in the hollow case. It could be easily improved to treat incomplete reconnection, but such a model would lack both experimental and numerical confirmation in the absence of reliable impurity density measurements and MHD codes able to simulate incomplete sawtooth crashes.

ACKNOWLEDGMENTS

This work was carried out within the framework of the European Fusion Development Agreement and the French Research Federation for Fusion Studies. It was supported by the European Communities under the contract of Association between Euratom and CEA. The views and opinions expressed herein do not necessarily reflect those of the European Commission. We acknowledge that the results in this paper have been achieved using HPC resources from GENCI-IDRIS (Grant No. 2013-t2013050198), GENCI-CURIE (Grant No. 2013-056348), and from the Mésocentre d'Aix-Marseille Université (Grant No. 2013-13b010).

[1]T. Pütterich, R. Dux, M. N. A. Beurskens, V. Bobkov, S. Brezinsek, J. Bucalossi, J. W. Coenen, I. Coffey, A. Czarnecka, C. Giroud, E. Joffrin, K. D. Lawson, M. Lehnen, E. de la Luna, J. Mailloux, S. Marsen, M.-L. Mayoral, A. Meigs, R. Neu, F. Rimini, M. Sertoli, M. Stamp, G. van Rooij, and JET EDFA Contributors, in 24th IAEA Fusion Energy Conference, San Diego, USA, 2012.
[2]T. Pütterich, R. Neu, R. Dux, A. Whiteford, M. O'Mullane, H. Summers, and ASDEX Upgrade Team, Nucl. Fusion 50, 025012 (2010).
[3]R. Dux, A. Peeters, A. Gude, A. Kallenbach, R. Neu, and ASDEX Upgrade Team, Nucl. Fusion 39, 1509 (1999).

[4]M. Nave, J. Rapp, T. Bolzonella, R. Dux, M. Mantsinen, R. Budny, P. Dumortier, M. von Hellermann, S. Jachmich, H. Koslowski, G. Maddison, A. Messiaen, P. Monier-Garbet, J. Ongena, M. Puiatti, J. Strachan, G. Telesca, B. Unterberg, M. Valisa, P. de Vries, and Contributors to JET-EFDA work programme, Nucl. Fusion 43, 1204 (2003).
[5]M. E. Puiatti, M. Valisa, M. Mattioli, T. Bolzonella, A. Bortolon, I. Coffey, R. Dux, M. von Hellermann, P. Monier-Garbet, M. F. F. Nave, J. Ongena, and Contributors to EFDA-JET work programme, Plasma Phys. Controlled Fusion 45, 2011 (2003).
[6]P. Belo, V. Parail, G. Corrigan, D. Heading, W. Houlberg, P. Monier-Garbet, J. Ongena, and JET EFDA Contributors, Plasma Phys. Controlled Fusion 46, 1299 (2004).
[7]T. Nakano, N. Asakura, H. Kubo, J. Yanagibayashi, and Y. Ueda, Nucl. Fusion 49, 115024 (2009).
[8]R. Dux, C. Giroud, R. Neu, A. Peeters, J. Stober, K.-D. Zastrow, and Contributors to EFDA-JET work programme, J. Nucl. Mater. 313–316, 1150 (2003); A. Grosman, "Plasma-surface interactions in controlled fusion devices," Nucl. Fusion 35, 1016 (1995).
[9]K. Tomabechi, J. Gilleland, Y. Sokolov, R. Toschi, and ITER Team, Nucl. Fusion 31, 1135 (1991).
[10]M. Redi, S. Cohen, and E. Synakowski, Nucl. Fusion 31, 1689 (1991).
[11]S. Chang, G. Miley, and C. Singer, Fusion Technol. 33, 387 (1998).
[12]T. Nicolas, R. Sabot, X. Garbet, H. Lutjens, J.-F. Luciani, Z. Guimaraes-Filho, J. Decker, and A. Merle, Phys. Plasmas 19, 112305 (2012).
[13]T. Nicolas, R. Sabot, H. Lütjens, J.-F. Luciani, R. Guirlet, J. Decker, A. Sirinelli, and JET-EFDA-Contributors, in 40th EPS Conference on Plasma Physics, Espoo, Finland, 2013.
[14]H. Lütjens and J.-F. Luciani, J. Comput. Phys. 229, 8130 (2010).
[15]B. Kadomtsev, Rep. Prog. Phys. 50, 115 (1987).
[16]I. Furno, C. Angioni, F. Porcelli, H. Weisen, R. Behn, T. Goodman, M. Henderson, Z. Pietrzyk, A. Pochelon, H. Reimerdes, and E. Rossi, Nucl. Fusion 41, 403 (2001).
[17]F. Porcelli, E. Rossi, G. Cima, and A. Wootton, Phys. Rev. Lett. 82, 1458 (1999).
[18]F. Halpern, H. Lütjens, and J.-F. Luciani, Phys. Plasmas 18, 102501 (2011).
[19]F. Halpern, D. Leblond, H. Lütjens, and J.-F. Luciani, Plasma Phys. Controlled Fusion 53, 015011 (2011).
[20]K. Krieger, T. Lunt, R. Dux, A. Janzer, A. Kallenbach, H. Mller, R. Neu, T. Ptterich, and V. Rohde, J. Nucl. Mater. 415, S297 (2011).
[21]M. Mattioli, C. D. Michelis, and A. Pecquet, Nucl. Fusion 38, 1629 (1998).
[22]R. Guirlet, D. Villegas, T. Parisot, C. Bourdelle, X. Garbet, F. Imbeaux, D. Mazon, and D. Pacella, Nucl. Fusion 49, 055007 (2009).
[23]J. D. Huba, *NRL Plasma Formulary* (Naval Research Laboratory, Washington DC, 2007).
[24]ITER Physics Basis Editors, Nucl. Fusion 39, 2137 (1999).
[25]R. Guirlet, A. Sirinelli, T. Parisot, R. Sabot, J. F. Artaud, C. Bourdelle, X. Garbet, P. Hennequin, G. T. Hoang, F. Imbeaux, J. L. Segui, D. Mazon, and D. Villegas, Nucl. Fusion 50, 095009 (2010).
[26]X. Garbet, P. Mantica, F. Ryter, G. Cordey, F. Imbeaux, C. Sozzi, A. Manini, E. Asp, V. Parail, R. Wolf, and JET EFDA Contributors, Plasma Phys. Controlled Fusion 46, 1351 (2004).
[27]J. A. Wesson, B. Alper, A. W. Edwards, and R. D. Gill, Phys. Rev. Lett. 79, 5018 (1997).
[28]T. Pütterich, R. Neu, R. Dux, A. Whiteford, M. O'Mullane *et al.*, Plasma Phys. Controlled Fusion 50, 085016 (2008).
[29]K. Wenzel and D. Sigmar, Nucl. Fusion 30, 1117 (1990).
[30]C. Angioni and A. G. Peeters, Phys. Rev. Lett. 96, 095003 (2006).
[31]M. Barnes, F. I. Parra, and W. Dorland, Phys. Rev. Lett. 109, 185003 (2012).
[32]F. Porcelli, D. Boucher, and M. Rosenbluth, Plasma Phys. Controlled Fusion 38, 2163 (1996).
[33]K. Asmussen, K. Fournier, J. Laming, R. Neu, J. Seely, R. Dux, W. Engelhardt, J. Fuchs, and ASDEX Upgrade Team, Nucl. Fusion 38, 967 (1998).
[34]C. G. Gimblett and R. J. Hastie, Plasma Phys. Controlled Fusion 36, 1439 (1994).
[35]J. Graves, I. Chapman, S. Coda, M. Lennholm, M. Albergante, and M. Jucker, Nat. Commun. 3, 624 (2012).
[36]I. T. Chapman, Plasma Phys. Controlled Fusion 53, 013001 (2011).
[37]A. Zocco, J. W. Connor, C. G. Gimblett, and R. J. Hastie, Plasma Phys. Controlled Fusion 55, 074005 (2013).
[38]Y. I. Kolesnichenko, Y. V. Yakovenko, D. Anderson, M. Lisak, and F. Wising, Phys. Rev. Lett. 68, 3881 (1992).
[39]D. Biskamp and J. F. Drake, Phys. Rev. Lett. 73, 971 (1994).
[40]J. Wesson, Plasma Phys. Controlled Fusion 28, 243 (1986).
[41]A. W. Edwards, D. J. Campbell, W. W. Engelhardt, H. U. Fahrbach, R. D. Gill, R. S. Granetz, S. Tsuji, B. J. D. Tubbing, A. Weller, J. Wesson, and D. Zasche, Phys. Rev. Lett. 57, 210 (1986).
[42]Y. Nagayama, K. M. McGuire, M. Bitter, A. Cavallo, E. Fredrickson, K. Hill, H. Hsuan, A. Janos, W. Park, G. Taylor, and M. Yamada, Phys. Rev. Lett. 67, 3527 (1991).